Supplementary Information

Membrane remodeling of Human Engineered Cardiac Tissue by Chronic Electric Stimulation

Alberto Sesena-Rubfiaro[1], Navin J. Prajapati[1], Lia Paolino[2], Lihua Lou[3], Daniel Cotayo[1], Popular Pandey[1], Mohammad Shaver[2], Joshua D. Hutcheson[2,4], Arvind Agarwal[3], Jin He[1,4*]

[1]Department of Physics, Florida International University, Miami, FL 33199, USA
[2]Department of Biomedical Engineering, Florida International University, Miami, FL 33199, USA
[3]Department of Mechanical and Materials Engineering, Florida International University, Miami, FL 33199, USA
[4]Biomolecular Science Institute, Florida International University, Miami FL 33199, USA
*corresponding author

Table of Contents

S1. The stiffness of the flexible PDMS post

To acquire the transmitted light optical microscope images, the hECTs were removed from the incubator and placed on a trinocular inverted microscope (AmScope, IN200TB) with 4x magnification. Bright-field videos were recorded at room temperature at 15 frames per second by a CCD camera (FLIR, Grasshopper3 GS3-U3-15S5M) for 10 s. After recording, the ECTs were quickly placed back into the incubator for the next day's recordings.

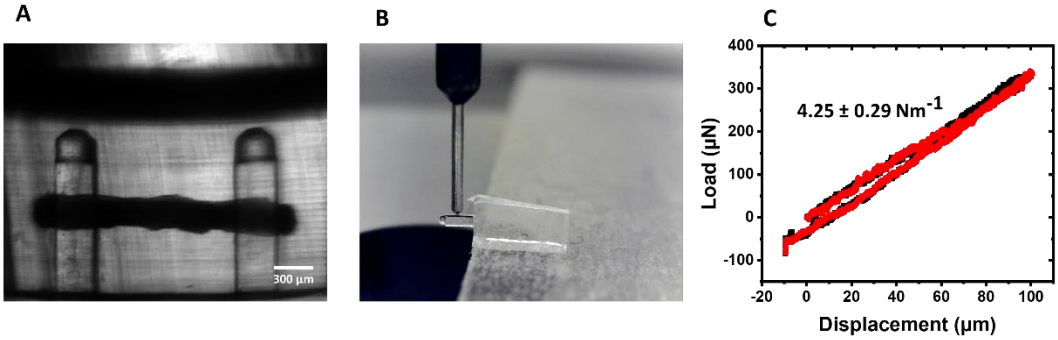

Figure S1: (A) Representative side-view image (transmitted light optical microscope image) of the hECT suspended between two flexible posts in the milli-tug device. The hECT normally stays at the middle of the post. (B) Mechanical testing of a PDMS post fabricated at 25:1 ratio of base: curing agent. To be consistent with the anchoring point of the hECT on the post, the test was conducted at the middle of the post. (C) Least-squares fitting of a representative loading and unloading curve of the indentation process on the PDMS post.

S2. FEM simulation

Numerical simulation was performed by using the software package COMSOL Multiphysics 5.2 assuming steady-state for simplification. Table S1 lists the FEM simulation parameters and Table S2 lists the boundary conditions.

Table S1: FEM simulation parameters

Parameters	Value
Diffusion Coefficient (K^+)	$1.957\mathrm{x}10^{-9}\ \mathrm{m}^2/\mathrm{s}$
Diffusion Coefficient (Cl^-)	$2.023\mathrm{x}10^{-9}\ \mathrm{m}^2/\mathrm{s}$
Charge number $(\mathrm{Z}_{\mathrm{K}^+})$	1
Charge number $(\mathrm{Z}_{\mathrm{Cl}^-})$	-1
Universal Gas Constant R	$8.3144621\ \mathrm{J/mol} * \mathrm{K}$
Relative Permittivity	80
Temperature T	298 K
Faraday Constant	$96485\ \mathrm{C/mol}$

Table S2: FEM boundary conditions

Gauss's and Faraday's law equations	steady-state
Surface charge density of PDMS	$\varphi_S = 0\ \mathrm{C/m}^2$
Surface charge density of 1xPBS	$\varphi_S = 0\ \mathrm{C/m}^2$
Ground voltage	$V = 0\ \mathrm{V}$
Voltage applied	$V = 13\ \mathrm{V}$
Relative permittivity graphite	12
Electrical conductivity graphite	$3x10^3\ S/m$
Relative permittivity silicone	3.5
Relative permittivity of 1xPBS	80
Electrical conductivity of 1xPBS	$1.6\ S/m$

S3. Comparison of the electrical stimulation setups

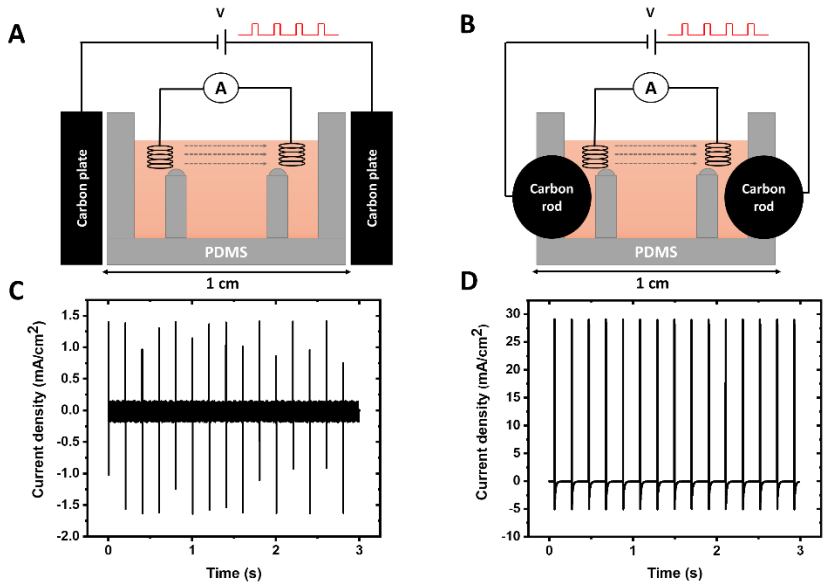

Figure S3: (A, B) The diagrams of the electrical current density measurement setup. Two Ag/AgCl wire electrodes in spiral shape were connected to a low noise current amplifier (DLPCA-200, FEMTO) to measure the current density in capacitive and direct current configurations, respectively. Two carbon electrodes provide a uniform electric field using monophasic square wave pulses of 13 V/cm amplitude and 2 ms width at 5 Hz frequency. (C, D) Representative recordings of the current density-time traces.

S4. The t-tubule structure revealed by WGA stained cross-sectioned hECT slices

We have conducted the Wheat Germ Agglutinin (WGA) staining experiments on the cross-sectioned tissue slices to reveal the lipid membrane structures of the tissue. The hECTs were first fixed by gradually increasing the concentration of paraformaldehyde (2%-4% in 1% increase, 30 min). Then the fixed hECT was embedded in optimal cutting temperature compound (OCT compound, Fisher scientific, 23-730-571) prior to frozen sectioning by a microtome-cryostat. The 10 μm thick cross-sectioned hECT slices were stained with WGA-Alexa Fluor 488 (Life Technologies, W11261) for 10 min, followed by rinsing in 1xPBS for 5 min. A few representative fluorescence images of the WGA stained cross-sections are shown in Figure S3A. We typically observed two continuous layers of lipid membranes, revealing the connected cells aligned at the outer surface of the tissue. When zoom-in the outer surface, we also found the T-tubule structures. We also compared the normalized fluorescence intensity of WGA and higher intensity was observed for hECTs under electrical stimulation both at days 8 and 16 (see Figure S3B).

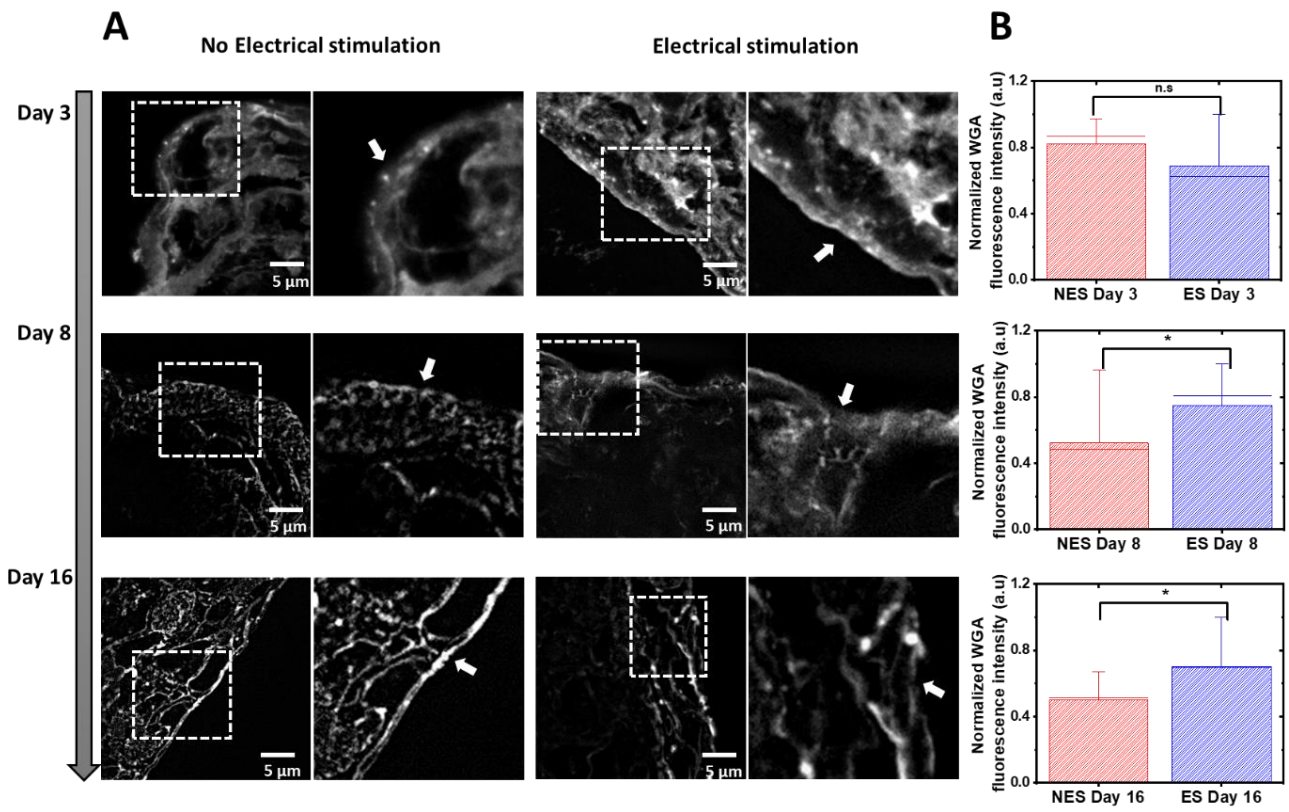

Figure S4. Effect of ES on the formation of the t-tubule network near the outer surface of the tissue. Representative images of the cross-sections of the hECT stained with WGA showing the t-tubule at different days of maturation without and without ES. White arrows in the zoom in images indicate the formation of the t-tubule from the surface towards the axis of hECT section. (B) The statistical analysis of the WGA fluorescence intensity (normalized to the background intensity) from two samples per day and between five to six repeats per sample. The error bar is the standard deviation.

S5. Patch-clamp experiments

The intracellular solution (pH 7.2) was prepared with the following composition: NaCl 8 mM, KCl 132.5 mM, $MgCl_2$ 2 mM, HEPES 10 mM. Tyrode or bath solution was prepared as previously described. Freshly cleaned borosilicate glass capillaries with filament (O.D. 1 mm, I.D. 0.58 mm, Sutter Instruments USA) were used to prepare nanopipettes (with typical pore size 200 nm) by a laser pipette puller (P-2000, Sutter Instruments, Novato, CA) with the following parameters: HEAT = 285, FIL = 4, VEL = 50, DEL = 200, PUL = 100. Burleigh PCS-5000 series micromanipulator with sub 100 nm resolution was used to control the motion of the nanopipette tip. The nanopipette tip was approached to slightly touch the tissue surface, similar to the operation on the single cell. The cardiac action potential recordings were performed at 25°C in a current-clamp configuration using the Axopatch 200B amplifier (Molecular Devices, San Jose, CA). Digidata 1440A controlled by the software Axoscope 10.5 (Molecular Devices) was used for the data acquisition. Representative recordings on the surface of the hECT are shown in Figure S4. Because the higher impedance of the nanopipette than the micropipette, the magnitude of the action potential spike is smaller. We have conducted the measurements at several random selected locations on the tissue surface and the successful rate is very high.

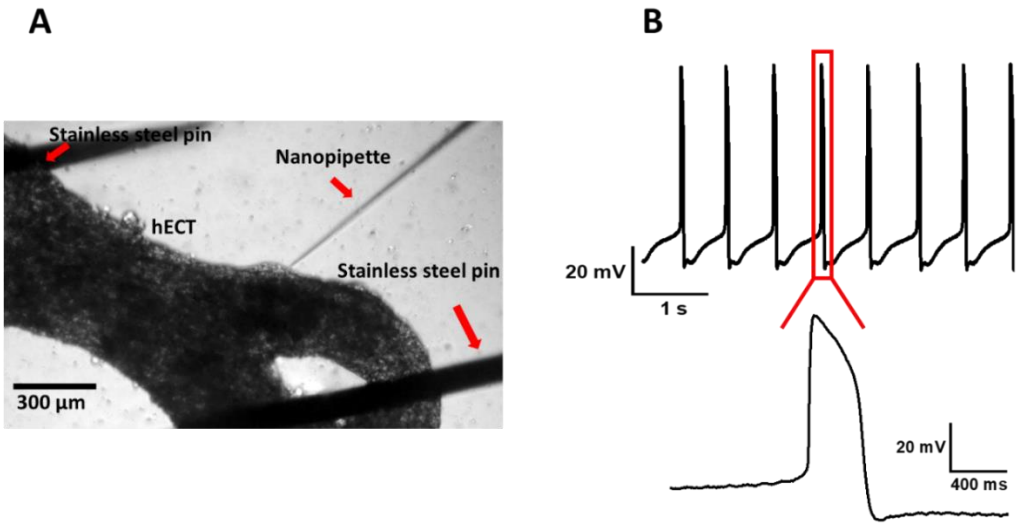

Figure S5. Whole cell patch-camp recording of the spontaneous action potentials from a live hECT at day 6 without ES. (A) The bright field image (with transmitted light) of a beating hECT supported by two stainless steel pins on a PDMS-coated plate after been removed from the flexible posts. The nanopipette only slightly touch the outer surface of the tissue. (B) Representative recording on the surface of the hECT (Top). The magnified view of one action potential is shown at the Bottom.

S6.Immunofluorescence images of the hECT

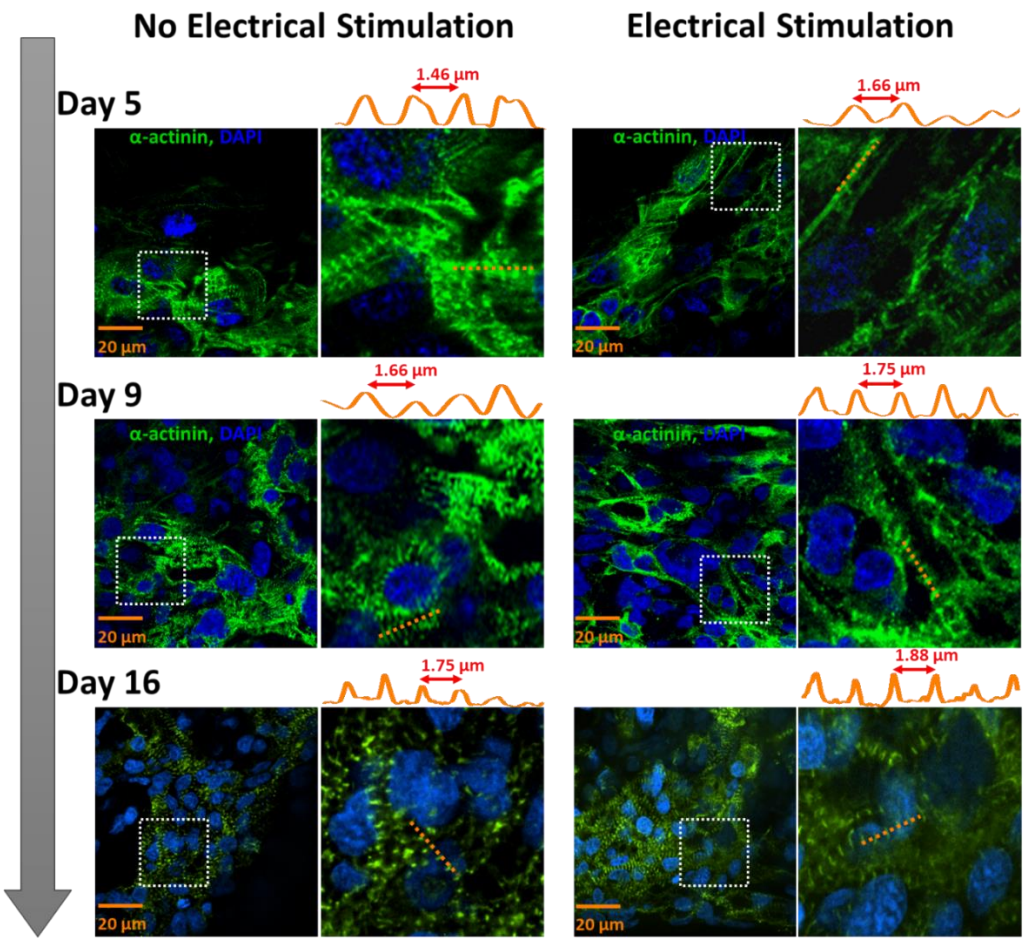

Figure S6. (A) Representative immunostained images of the structural organization in the hECT stained for α-actinin (green) and nucleus (blue). The intensity profiles along the orange dashed lines are shown on top of each fluorescence image.

S7. Fluorescence images and intensity of the calcium transients

Figure 4A in main text shows the intracellular calcium transients. The corresponding fluorescence images are shown in Figure S7A. The fluorescence intensity at the early stage of maturation (day 2) is generally not uniform and higher at the edge of tissue, suggesting the higher concentration of CMs near the tissue edge. In contrast, hECT at the late stage of maturation (day 11) shows more uniform fluorescence intensity distribution while the intensity at the edge is much lower compared with the tissue at day 2 (Figure S7B), revealing the migration of CMs towards the center of the hECT. At day 11, significant differences were found for the fluorescence intensity of the calcium transients between tissues with and without ES.

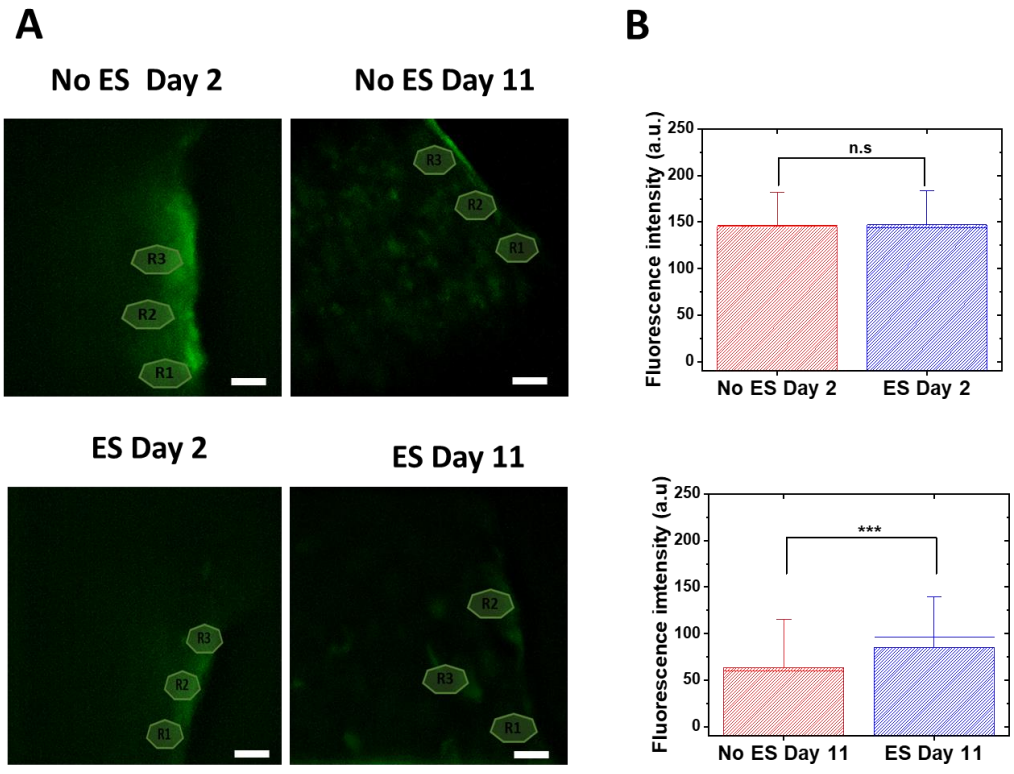

Figure S7. (A) Fluorescence images of the hECTs loaded with Fluo-4 during relaxation time. The white scale bar is 30 μm. (B)The statistical analysis of the amplitude of the fluorescence intensity (from baseline to the peak) from 50 calcium transients (from two samples per day and three repeats per sample). The error bar is the standard deviation.

S8. The temperature effect to the beating frequency of tissue

It is important to notice that the measurement temperature can strongly affect the measured beating frequency. The beating frequency is lower when the environment temperature is lower. Here we showed the twitch force-time traces of tissues recorded on day 4 and 11 at 32°C (see Figure S8). Without ES, the beating frequency of hECT decreases from 66 beats per minute (bpm) at day 4 to 60 bpm at day 11. With ES, the beating frequency decreases even more obviously from 60 bpm at day 4 to 48 bpm at day 11. In contrast, the twitch force magnitude was not strongly affected by the temperature.

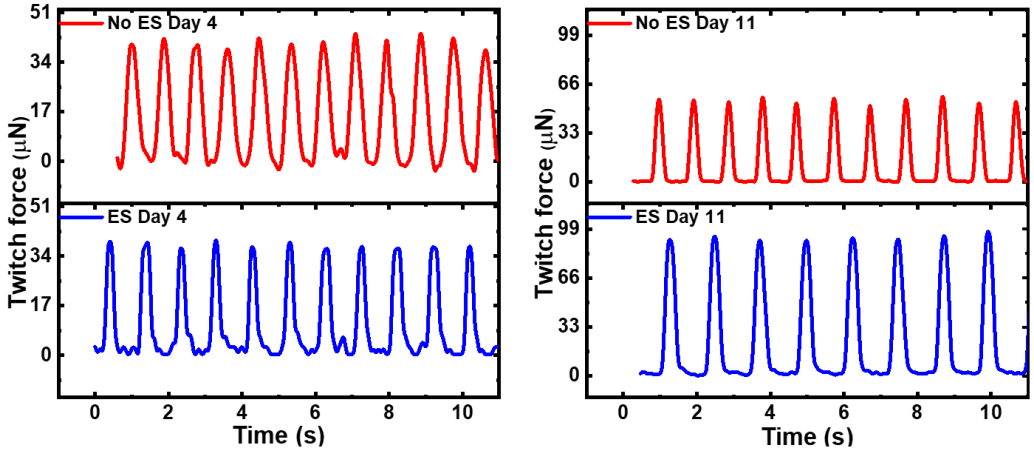

Figure S8. Recordings of the twitch force-time traces of tissues recorded on days 4 and 11 at 32°C without (red color) and with ES (blue color).

S9. Geometrical changes of the hECTs

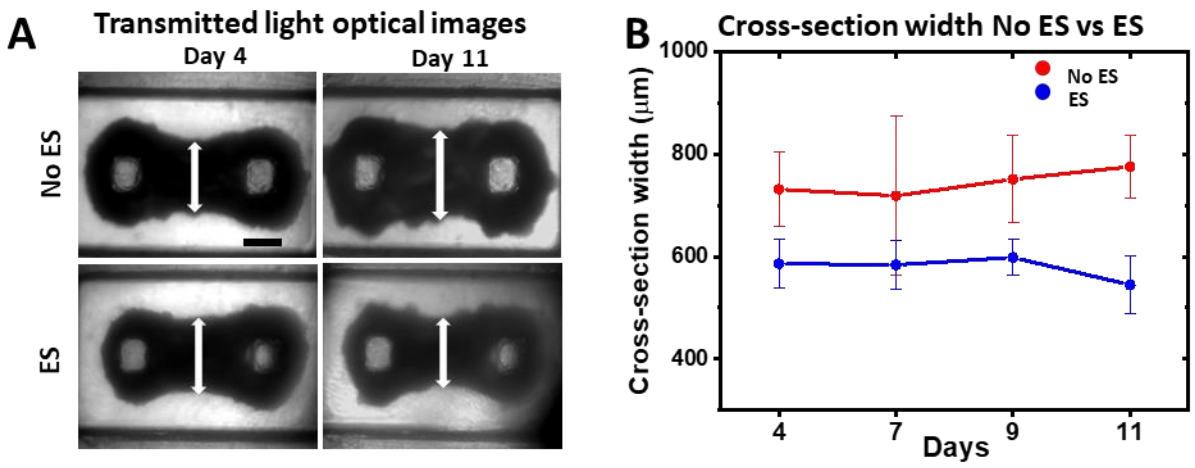

Figure S9. (A) Bright-field images of the hECTs without (top row) and with (bottom row) ES in transmission mode at day 4 and day 11 of culture. The black scale bar is 500 μm. (B) The change of cross-section width of the tissue (denoted by the solid white lines in the optical images) with culture time. The error bars are calculated from the standard deviation of 5 different hECTs (N=5).

S10. The analyzed volume nuclei/sarcomere ratio

We have found the tendency of increased sarcomere appeared in the fluorescence image. We quantify the sarcomere change by using the volume nuclei/sarcomere ratio. To calculate the volume nuclei/sarcomere ratio, the z-stacks (containing 30 images) of confocal fluorescence images were segmented by the intensity threshold to compute the occupied area of nuclei (stained by DAPI) and sarcomere (stained to α-actinin) in each image. The volume was obtained by summing the product of area and the depth between images of multiple images. Compared with the day 3 tissue, we found significantly higher ratio from the tissue without ES at day 11, implying the increased fraction of sarcomere in the day 11 tissue with ES.

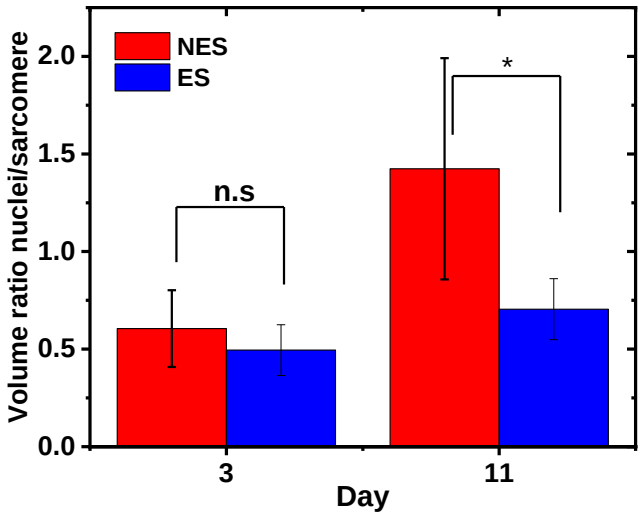

Figure S10. The volume nuclei/sarcomere ratio for day 3 and day 11 tissues with (blue) and without ES treatment (red). The ratio was obtained from two z-stack images per sample for each condition.

S11. The morphology of the isolated cells from the day 16 tissues

To better the morphology of individual cells in the tissue, we isolated some cells from the day 16 tissues. The hECTs were dissociated into single cardiomyocytes by using papain-base solution containing 20 U/ml of papain enzyme (Sigma-Aldrich 76220), 1.1 mM EDTA and 5.5 mM l-Cysteine-HCL (Sigma-Aldrich C7880), diluted in 1xEBSS (Gibco 24010-043). The hECTs were continuous stirred in papain-base solution at 35°C for 10 min. The papain activity was fished by adding DMEM (Corning 10013CV) supplemented with 10 % FBS (Gibco 26140079). The solution was centrifuged at 800 RPM for 5 min at 25 °C. Then, the yielded pellet was resuspended in RPMI/B27 containing insulin, 5 µM Y27632 (Tocris, 1254) and 10% FBS. The PDMS silanized cell culture plates were treated with 10 µg ml^{-1} of human fibronectin (Gibco 33016-015) for 1 hr at 35°C and rinsed with sterile 1xPBS. The isolated CMs were replanted on the fibronectin coated PDMS cell culture plate and stored in a cell culture incubator (37°C, 5%, CO_2, 90% humidity) before measurements.

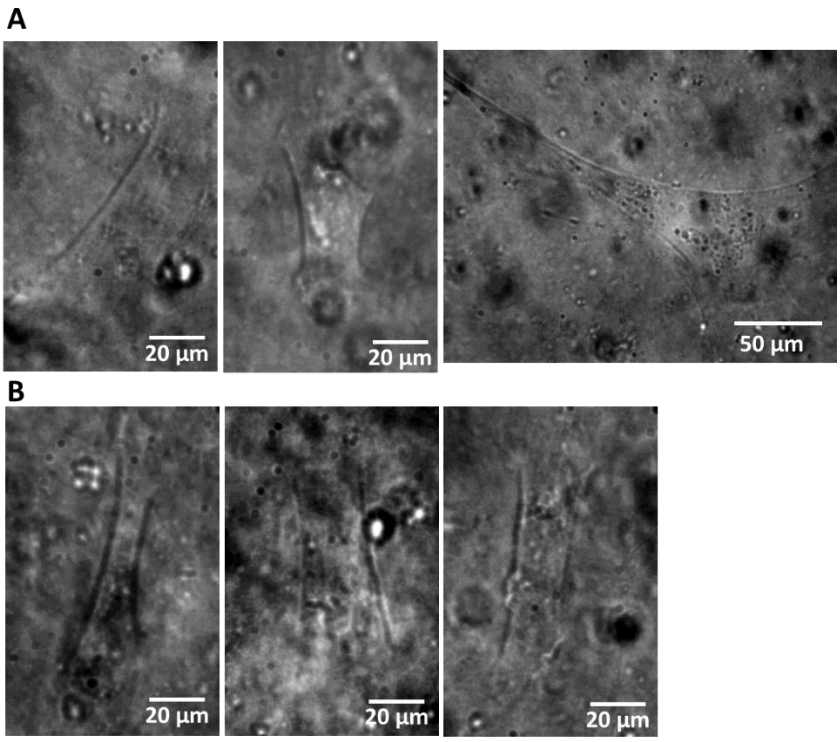

Figure S11. The bright-field images of isolated cells from day 16 hECTs. (A) The cells isolated from hECTs without electrical stimulation show more variations in their geometrical shape. (B) The cells isolated from hECTs with electrical stimulation show more uniform and more elongated shape.

S12. The nanoindentation measurement

The method: The micromechanical properties of live hECTs in the milli-tug construct submerged in the tissue culture medium were measured by the indentation technique (Hysitron Biosoft, Bruker, Billerica, MA) at room temperature. A diamond conospherical fluid cell probe with a nominal radius of 50 μm was used. The test was conducted via the probe-tissue contact and displacement control modes with three programmed segments: loading, unloading, and retraction. The initiation of indentation testing with the probe-tissue contact method was applied to overcome the difficulty of surface detection under hydrated conditions. A high displacement control mode was chosen to account for the tissue surface roughness, sink-in effects, and adhesion challenges. The loading and unloading segments were set at 2 μm/s for 50 μm and -2 μm/s for -50 μm, respectively. The retraction was set at -5 μm/s for 30s to ensure the complete detachment of the probe after the loading-unloading cycle. The overall indentation process was recorded by a two-camera system: dino-lite and endoscope for the top and side views, respectively. The cameras were also used to capture initial probe-tissue contact and indentation position. The hECTs were measured using this method at 2, 5, 9, and 11 days of culture. The measurements of each tissue sample were repeated at least three times. The buoyancy correction was applied on raw load-displacement data to eliminate the effects of tissue culture medium on the probe. The Hertzian contact model was used to analyze the elastic deformation of tissues, where elastic modulus (E, MPa) was calculated based on equation S1.

$$F = \frac{4}{3}\frac{E}{1-\mu^2}\sqrt{R{\delta_0}^3} \qquad \text{(Equation S1)}$$

F, μ, R, and δ_0 are applied force (μN), the Poisson's ratio, radius of the probe, and the indentation depth.

Results: We conducted indentation measurements on the hECTs to probe their mechanical changes as a function of culture time. A top view of the indentation probe on the hECT in the milli-tug construct is shown in Figure S12A. A schematic diagram of the indentation measurement is illustrated in Figure S12B, where the diamond indenter probe was always targeted at the center of the tissue. The obtained load-displacement curves for a 5-day hECT without ES are presented in Figure S12C, which indicates the consistency of the three repeats and the robustness of the indentation method. The load-displacement curve exhibited noise in data points compared to the smooth curves of stiff materials (*e.g.*, graphene foam/polymer hybrid, mushroom bio-leather, and metal matrix [1]), which might be attributed to the viscoelastic properties. Viscoelasticity is a time-dependent characteristic because of the temporary interconnection and diffusion among the adjacent long molecules within tissues.

Based on the load-displacement curve (Figure S12C), we calculated the elastic modulus (Young's modulus) of the hECT at different culture days without and with ES. The results are shown in Figure S12D. The average elastic modulus of hECT without and with ES exhibited ranges of 2.68-4.72 kPa and 3.48-4.99 kPa, respectively. Previous reports on ECTs composed of CMs and endothelial cells presented Young's modulus 4-5 kPa.[2] Moreover, the range of human heart tissue and hiPSC-derived hECT stiffness or elastic modulus is 2-100 kPa based on previous research studies.[3] The wide range might be attributed to tissue location/composition effects, sample size/source, physical stimulus, and measuring equipment/method. Therefore, the comparatively low elastic modulus of

our hECTs might associate with the simplified tissue composition (mainly CMs and fibrin/Matrigel ECM), compared to the more complex compositions of native human cardiac tissues (CMs, fibroblasts, smooth muscle cells, thin/thick filaments, blood vessels, and more complexed ECM). As known, the stiffness of the ECM mainly formed by fibrin/matrigel is also relatively low.[4] Noticeably, the hECTs with ES demonstrated higher mean values of elastic modulus consistently. However, due to the big sample-to-sample fluctuation, we only found statistical significant difference with and without ES for day 7 tissue and the differences are not conclusive for other days.

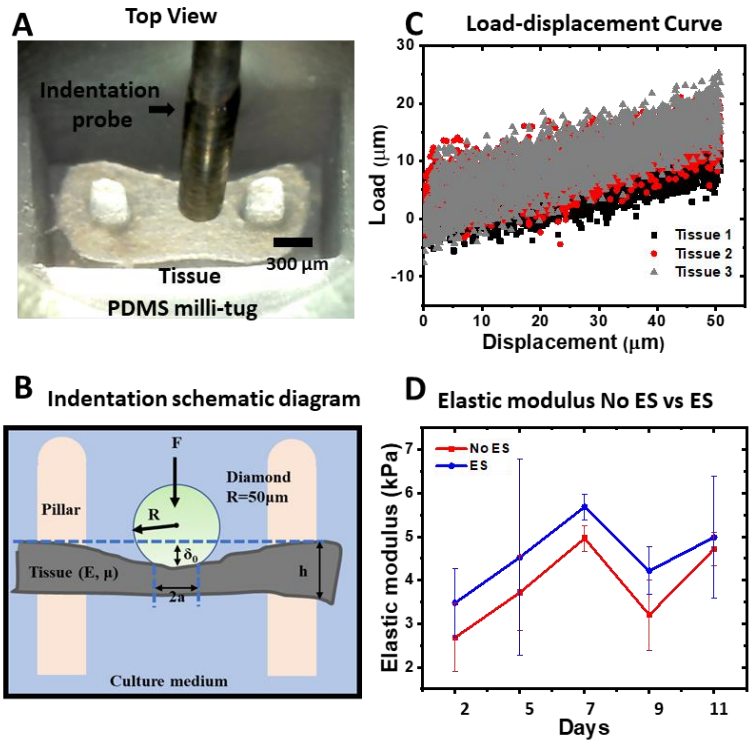

Figure S12. Mechanical changes of the hECTs. (A) Top view of the indentation process. (B) Indentation schematic diagram. (C) Load-displacement curve (load-unload) for three day-5 hECTs without ES. All the load-displacement curves were after buoyancy correction. (D) Elastic modulus of the hECTs with and without ES as a function of culture

days. The error bars are calculated from the standard deviation of 6 measurements (three samples per day and two repeats per sample).

The increase of elastic modulus with the culture time is also not monotonic. An increase in elastic modulus was observed from days 2 to 7, but a decrease was observed between days 7 and 9. After day 9, the elastic modulus increases again. The trend is consistent with the twitch force results in Figure S12D. The overall measured mechanical changes over time are presumably attributed to the chronical structural changes in the hECT generated by the cell growth and migration in ECM and the cell-ECM interactions.

References

(1) Paul, T.; Zhang, C.; Boesl, B.; Agarwal, A. Correlations to Predict Microstructure and Mechanical Properties of Ultrasonically Cast Metal Matrix Nanocomposites as a Function of Treatment Time. *Advanced Engineering Materials* **2020**, *22* (10), 2000413, https://doi.org/10.1002/adem.202000413. DOI: https://doi.org/10.1002/adem.202000413 (acccessed 2021/05/01).

(2) Masumoto, H.; Nakane, T.; Tinney, J. P.; Yuan, F.; Ye, F.; Kowalski, W. J.; Minakata, K.; Sakata, R.; Yamashita, J. K.; Keller, B. B. The myocardial regenerative potential of three-dimensional engineered cardiac tissues composed of multiple human iPS cell-derived cardiovascular cell lineages. *Scientific Reports* **2016**, *6* (1), 29933. DOI: 10.1038/srep29933.

(3) Hasan, A.; Ragaert, K.; Swieszkowski, W.; Selimović, Š.; Paul, A.; Camci-Unal, G.; Mofrad, M. R. K.; Khademhosseini, A. Biomechanical properties of native and tissue engineered heart valve constructs. *Journal of Biomechanics* **2014**, *47* (9), 1949-1963. DOI: https://doi.org/10.1016/j.jbiomech.2013.09.023. Lee, S.; Serpooshan, V.; Tong, X.; Venkatraman, S.; Lee, M.; Lee, J.; Chirikian, O.; Wu, J. C.; Wu, S. M.; Yang, F. Contractile force generation by 3D hiPSC-derived cardiac tissues is enhanced by rapid establishment of cellular interconnection in matrix with muscle-mimicking stiffness. *Biomaterials* **2017**, *131*, 111-120. DOI: https://doi.org/10.1016/j.biomaterials.2017.03.039. Engler, A. J.; Griffin, M. A.; Sen, S.; Bönnemann, C. G.; Sweeney, H. L.; Discher, D. E. Myotubes differentiate optimally on substrates with tissue-like stiffness : pathological implications for soft or stiff microenvironments. *Journal of Cell Biology* **2004**, *166* (6), 877-887. DOI: 10.1083/jcb.200405004 (acccessed 5/1/2021).

(4) Kaiser, N. J.; Kant, R. J.; Minor, A. J.; Coulombe, K. L. K. Optimizing Blended Collagen-Fibrin Hydrogels for Cardiac Tissue Engineering with Human iPSC-derived Cardiomyocytes. *ACS Biomaterials Science & Engineering* **2019**, *5* (2), 887-899. DOI: 10.1021/acsbiomaterials.8b01112. Aisenbrey, E. A.; Murphy, W. L. Synthetic alternatives to Matrigel. *Nature Reviews Materials* **2020**, *5* (7), 539-551. DOI: 10.1038/s41578-020-0199-8.